Available online at www.sciencedirect.com
ScienceDirect
Trans. Nonferrous Met. Soc. China 28(2018) 1351−1359
Transactions of Nonferrous Metals Society of China
www.tnmsc.cn

Superelastic behavior of nanostructured $Ti_{50}Ni_{48}Co_2$ shape memory alloy with cold rolling processing

E. MOHAMMAD SHARIFI[1], A. KERMANPUR[2]

1. Department of Materials Engineering, Malek Ashtar University of Technology, Shahin Shahr 83145115, Iran;
2. Department of Materials Engineering, Isfahan University of Technology, Isfahan 8415683111, Iran

Received 21 May 2017; accepted 14 October 2017

Abstract: Effects of cold rolling followed by annealing on microstructural evolution and superelastic properties of the $Ti_{50}Ni_{48}Co_2$ shape memory alloy were investigated. Results showed that during cold rolling, the alloy microstructure evolved through six basic stages including stress-induced martensite transformation and plastic deformation of martensite, deformation twinning, accumulation of dislocations along twin and variant boundaries in martensite, nanocrystallization, amorphization and reverse transformation of martensite to austenite. After annealing at 400 °C for 1 h, the amorphous phase formed in the cold-rolled specimens was completely crystallized and an entirely nanocrystalline structure was achieved. The value of stress level of the upper plateau in this nanocrystalline alloy was measured as high as 730 MPa which was significantly higher than that of the coarse-grained $Ni_{50}Ti_{50}$ and $Ti_{50}Ni_{48}Co_2$ alloys. Moreover, the nanocrystalline $Ti_{50}Ni_{48}Co_2$ alloy had a high damping capacity and considerable efficiency for energy storage.

Key words: shape memory alloy; superelasticity; nanocrystalline material; thermomechanical processing

1 Introduction

Superelasticity refers to large recoverable deformation associated with stress-induced forward and reverse transformation occurred in shape memory alloys (SMAs) at constant temperature. The magnitude of such recoverable strain can be 20 times higher than the elastic strain of steels [1−4]. The superelastic properties of SMAs, such as the recovery and residual strains, the stress level of upper and lower plateaus, are all structure-sensitive. Therefore, various thermomechanical treatments causing a well-developed dislocation sub-structure or nanocrystalline structure are effectively used for improving the superelastic properties of SMAs [5−7]. TSUCHIA et al [8] produced nanocrystalline NiTi wire with high tensile strength and high elastic modulus. DELVILLE et al [9] and MALARD et al [10] prepared nanostructured NiTi wire by means of cold drawing and heat treatments. They found that the NiTi wire with nanocrystalline structure possesses the perfect superelasticity with a recoverable strain of 8%.

It is shown that the addition of Co in NiTi alloy may increase the loading and unloading plateaus and workability when compared with the binary NiTi alloy [11,12]. FASCHING et al [12] studied the effect of Co addition as a substitute for Ni on the stiffness and plateau stresses of a superelastic NiTi alloy and compared the mechanical properties of the TiNiCo with those of the binary NiTi alloy. It was found that $Ti_{50}Ni_{50-x}Co_x$ (x=1−2, mole fraction, %) alloys exhibited about 30% higher modulus, loading plateau, and unloading plateau as compared to the binary alloy [12]. JING and LIU [13] investigated the influence of Co addition (ranging from 2% to 10%) on the mechanical properties of NiTi alloy. It was found that the addition of Co resulted in high yield strength [13].

The tensile properties and transformation behavior of the nanostructured $Ti_{50}Ni_{48}Co_2$ shape memory alloy prepared by copper boat induction melting followed by thermomechanical treatment were discussed [14,15]. The present work attempted to investigate effects of the thermomechanical processing comprised of cold rolling followed by annealing on the superelastic properties of the nanocrystalline $Ti_{50}Ni_{48}Co_2$ shape memory alloy.

Corresponding author: E. MOHAMMAD SHARIFI; Tel: +98-3145912501; Fax: +98-3145228530; E-mail: ehsan_sharifi_2000@yahoo.com
DOI: 10.1016/S1003-6326(18)64773-9

2 Experimental

$Ti_{50}Ni_{48}Co_2$ (mole fraction, %) cast ingot was prepared by a copper-boat vacuum induction melting system. The ingot was homogenized at 900 °C for 4 h and then hot rolled at 900 °C into a sheet of 2.5 mm in thickness. The rolled sample was annealed at 900 °C for 1 h in vacuum followed by water quenching. The annealed specimens were cold rolled with 20%−70% thickness reduction at room temperature. Based on crystallization temperatures determined from calorimetric measurements, post deformation annealing was conducted at 400 °C for 1 h in vacuum.

Calorimetric analyses were performed by differential scanning calorimetry (DSC), using a NETZSCH 200F3 instrument with a heating–cooling rate of 10 °C/min. X-ray diffraction (XRD) was performed using a Philips X'Pert diffractometer with Cu K_α radiation. Transmission electron microscopy (TEM) observations were conducted in a JEOL−2100F instrument operated at 200 kV. Samples for TEM were prepared by polishing with a twin-jet electro-polisher (Struers, Tenupol−5) in a solution of 90% acetic acid glacial and 10% perchloric acid at 15 °C under 35 V.

The crystallite size, residual microstrain and dislocation density of all samples that were subjected to various cold reductions were determined by analyzing the XRD patterns via the Rietveld software, materials analysis using diffraction (MAUD) [16]. Details of analysis method have been reported elsewhere [16−19]. After fitting the theoretical curve on the XRD pattern of samples, related values of microstructural parameters (such as crystallite size and microstrain) for each XRD peak were provided by software. The value of the dislocation density (ρ) was calculated [20] from the average values of the crystallite size (D) and microstrain $(\varepsilon^2)^{0.5}$ (output data of MAUD software) by the following equation:

$$\rho = \frac{3\sqrt{2\pi}(\varepsilon^2)^{0.5}}{Db} \quad (1)$$

where b is the absolute value of Burgers vector.

Tensile test was carried out according to ASTM-F2516 (standard test method for tension testing of nickel-titanium superelastic materials) with a strain rate of 10^{-3} s^{-1} at room temperature. All tensile test specimens were cut along the rolling direction.

3 Results and discussion

3.1 Microstructural change and phase transformation during thermomechanical processing

The as-homogenized microstructure was composed of the coarse grained $B2$ austenite with an average size of 50 μm. According to DSC results, the homogenized $Ti_{50}Ni_{48}Co_2$ alloy had a two-stage transformation during cooling including the austenite to R phase and the R phase to martensite. The measured transformation temperatures of the homogenized $Ti_{50}Ni_{48}Co_2$ alloy are M_f=−18 °C, M_s=13 °C, R_f=20 °C, R_s=31 °C, A_s=17 °C and A_f=44 °C.

Cold rolling of $Ti_{50}Ni_{48}Co_2$ alloy led to significant peak broadening in X-ray diffraction pattern as a result of introduction of high density of dislocations and crystal refinement [21]. Peak broadening would also be related to the occurrence of amorphization as a result of subjecting the alloy to severe plastic deformation [22]. The average values of the crystallite size and microstrain of cold-rolled specimens with various thickness reductions which were calculated by MAUD software are given in Table 1. It is noticed that the cold rolling reduces the crystallite size and increases the microstrain.

The calculated values of dislocation density (from the data of Table 1 and Eq. (1)) are presented in Fig. 1. It can be seen that dislocation density is increased to 8.55×10^{12} cm^{-2} with increasing thickness reduction up to 70%. Similar results were reported by KOIKE et al [23]. They estimated an extremely high dislocation density of 10^{13} to 10^{14} cm^{-2} in cold-rolled NiTi. They suggested that

Table 1 Average values of crystallite size (D) and microstrain (ε) of cold-rolled specimens with various thickness reductions

Thickness reduction/%	D/Å	ε
20	62	0.00301
30	52	0.00452
40	46	0.00582
50	39	0.00683
60	37	0.00874
70	27	0.00914

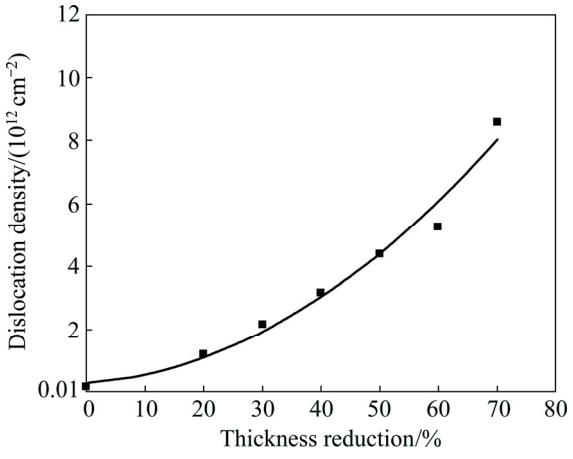

Fig. 1 Calculated dislocation density as function of thickness reduction in cold-rolled $Ti_{50}Ni_{48}Co_2$ specimens

this dislocation density is a major driving force for amorphization in cold-rolled NiTi.

Figure 2 shows the TEM image of the cold-rolled $Ti_{50}Ni_{48}Co_2$ specimen by 40% reduction with the corresponding selected area diffraction pattern (SADP). It can be seen that after 40% thickness reduction, a lamellar structure similar to the martensite deformation twinning structure is formed in the cold-rolled microstructure (Fig. 2(a)). However, the SADP shown in Fig. 2(b) indicates that the structure is mainly nano-crystalline *B*2 austenite and amorphous phase. Therefore, it can be inferred that the initial deformation mechanism of this alloy during cold rolling is stress-induced martensitic transformation followed by plastic deformation of martensite via dislocation slip and subsequent martensite to austenite transformation via the reverse transformation after cold rolling (unloading).

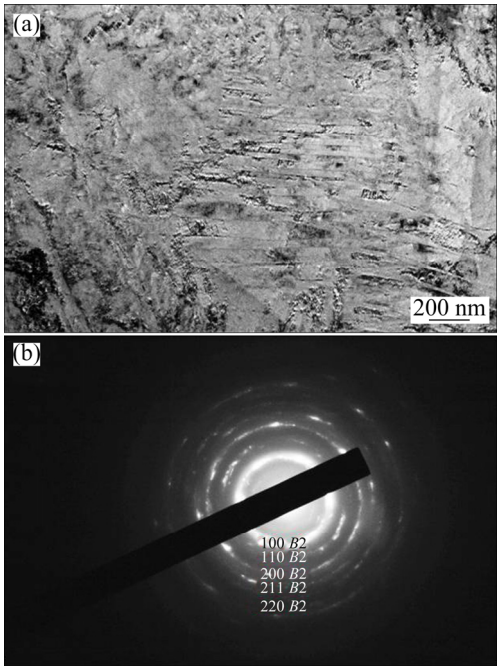

Fig. 2 Bright field TEM image (a) and corresponding diffraction pattern (b) of 40% cold-rolled $Ti_{50}Ni_{48}Co_2$ alloy

The twin boundaries in the martensite structure act as the blocking site for the motion of dislocations during the deformation and promote high density accumulation of dislocations [24]. Figure 3(a) shows a TEM image taken from a different position in the 40% cold rolled specimen showing a high density arrays of dislocations which seem to define original twin boundaries in the stress-induced martensite [14,15]. Moreover, the SADP in Fig. 3(b) confirms that this structure mainly consists of the nanocrystalline *B*2 phase. Therefore, it can be mentioned that along with the occurrence of high density accumulation of dislocations and the interaction between them, the cold-rolled specimen is gradually subjected to nanocrystallization with the help of the dislocation cells.

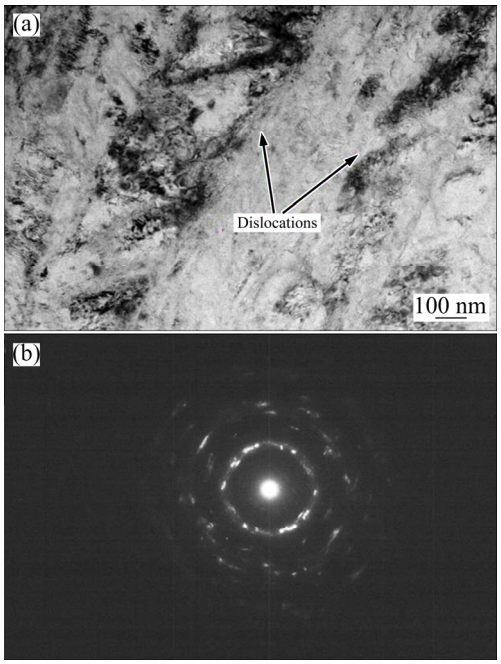

Fig. 3 Bright field TEM image (a) and corresponding diffraction pattern (b) taken from different positions in 40% cold-rolled specimen

By increasing the cold deformation, the dislocation density becomes greater than a critical value, beyond which the nanocrystalline phase is further subjected to amorphization [14,15,23]. Figure 4 shows TEM image and the SADP of the 70% cold-rolled $Ti_{50}Ni_{48}Co_2$ specimen. As seen in Fig. 4(a), the 70% cold-rolled specimen contains heterogeneously distributed nanocrystals that are embedded in the dominant amorphous matrix. The visible halo in the SADP (Fig. 4(b)) indicates the formation of the amorphous phase, while the continuous diffraction rings show the formation of nanocrystalline *B*2 phase.

In summary, with the consecutive increase of the plastic deformation, microstructural evolution of $Ti_{50}Ni_{48}Co_2$ alloy has six basic stages, namely stress-induced martensite transformation and plastic deformation of martensite, deformation twinning, accumulation of dislocations along twin and variant boundaries in martensite, nanocrystallization, amorphization and reverse transformation of martensite to austenite. Figure 5 shows schematic diagrams of deformation mechanisms of $Ti_{50}Ni_{48}Co_2$ alloy during cold rolling via this transformation sequence.

According to the crystallization temperatures determined from the DSC measurements, annealing treatment was performed at 400 °C for 1 h in vacuum in order to crystallize the amorphous phase in the cold-rolled specimens. TEM image and SADP of the 40% and 70% cold-rolled $Ti_{50}Ni_{48}Co_2$ specimens after annealing at 400 °C are shown in Figs. 6 and Fig. 7, respectively. A

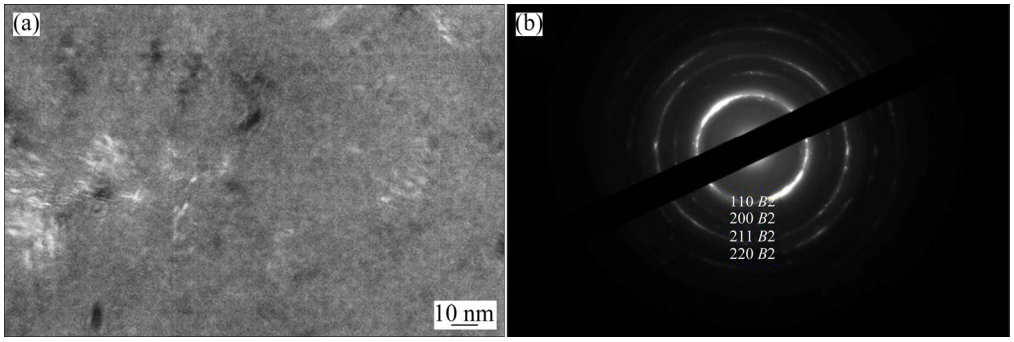

Fig. 4 Bright field TEM image (a) and corresponding diffraction pattern (b) of 70% cold-rolled $Ti_{50}Ni_{48}Co_2$ alloy

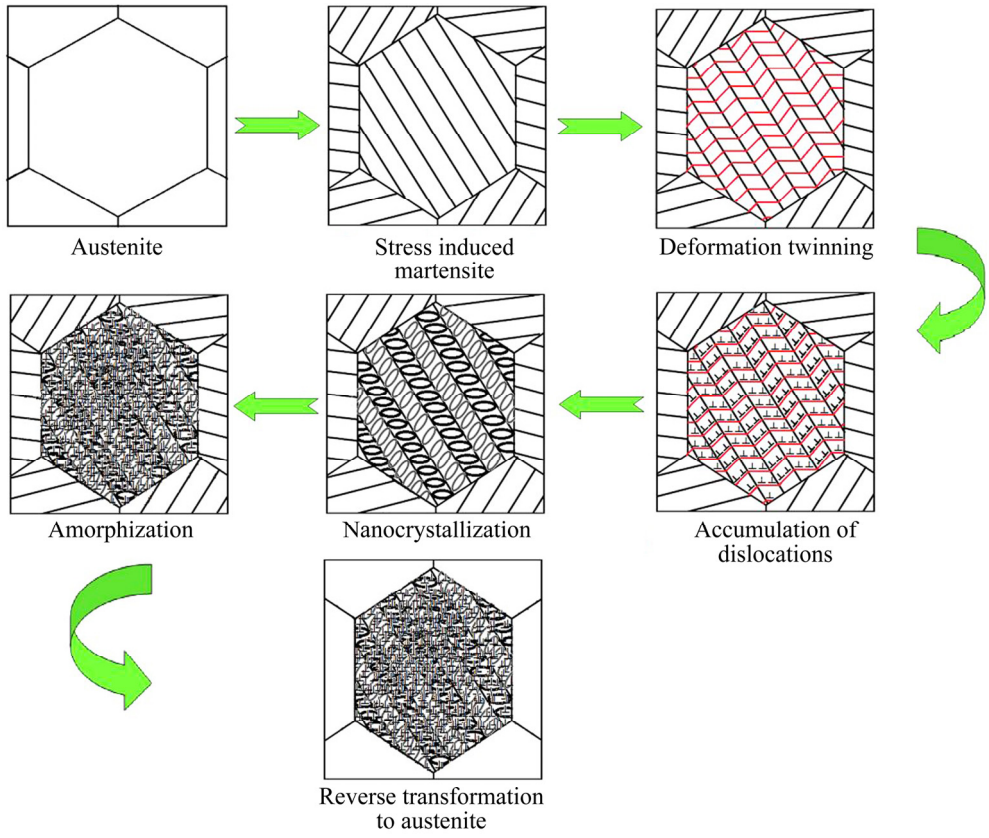

Fig. 5 Schematic diagram of deformation mechanisms of $Ti_{50}Ni_{48}Co_2$ alloy during cold rolling

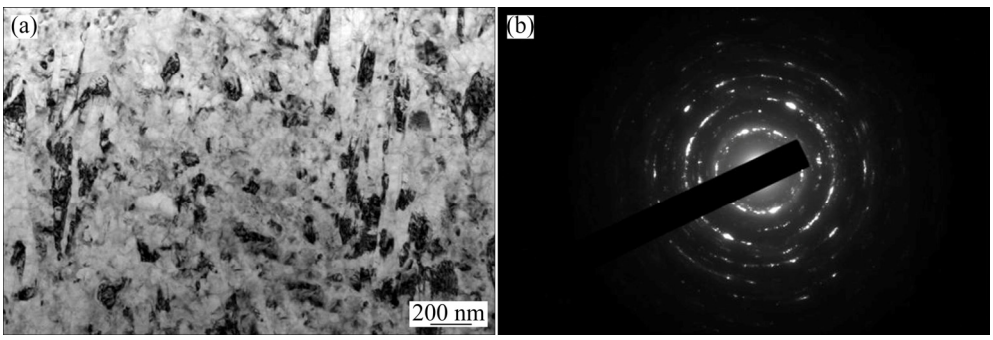

Fig. 6 Bright field TEM image (a) and SADP (b) of 40% cold-rolled $Ti_{50}Ni_{48}Co_2$ specimen after annealing at 400 °C for 1 h

nanocrystalline structure (as verified by its continuous diffraction rings) is clearly observed in the annealed specimens. The grain size of the 40% cold-rolled and annealed specimen is 10−110 nm (Fig. 6), whereas it is 5−60 nm for the 70% cold-rolled and annealed one (Fig. 7). This shows the correlation between the final

grain size and the thickness reduction during cold rolling prior to annealing treatment. For both specimens, the SADP pattern is identified as the austenite and martensite phases with no diffuse rings corresponding to the amorphous phase, showing the completion of crystallization. These are in agreement with the XRD results [14,15].

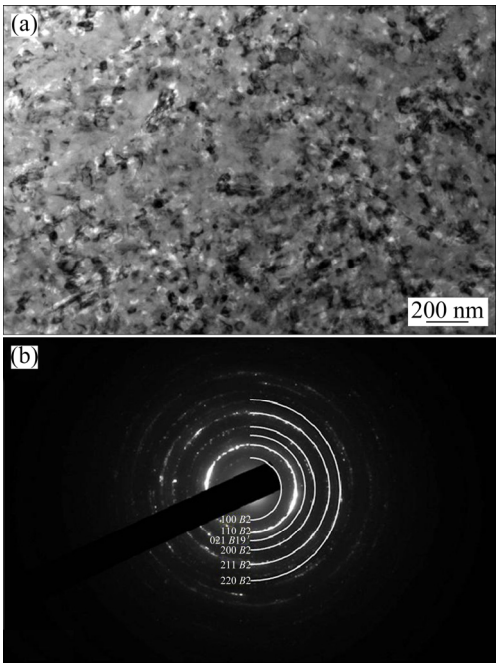

Fig. 7 Bright field TEM image (a) and SADP (b) of 70% cold-rolled $Ti_{50}Ni_{48}Co_2$ specimen after annealing at 400 °C for 1 h

Figure 8 illustrates the thermal transformation behaviors of the 40% and 70% cold-rolled $Ti_{50}Ni_{48}Co_2$ specimens annealed at 400 °C. Unlike the cold-rolled specimens whose DSC curves showed no transformation peak (not shown), annealed specimens exhibited a single-stage $B2 \rightarrow B19'$ transformation on cooling and a two-stage $B19' \rightarrow R \rightarrow B2$ transformation on heating. This implies that the post deformation annealing annihilates defects such as dislocations and vacancies generated during deformation which locked the austenite–martensite transformation interfaces and as a result the martensitic transformation emerges again in subsequent thermal cycles [14,15,21].

3.2 Superelastic behavior of nanocrystalline $Ti_{50}Ni_{48}Co_2$ alloy

Figure 9 illustrates tensile stress–strain curves of the $Ti_{50}Ni_{48}Co_2$ specimens cold rolled up to 70% followed by post deformation annealing at 400 °C. During loading, elastic deformation of austenite is observed up to the critical stress level for stress-induced martensitic transformation. Further loading results in austenite to martensite transformation which is associated with a plateau region and then subsequent elastic deformation

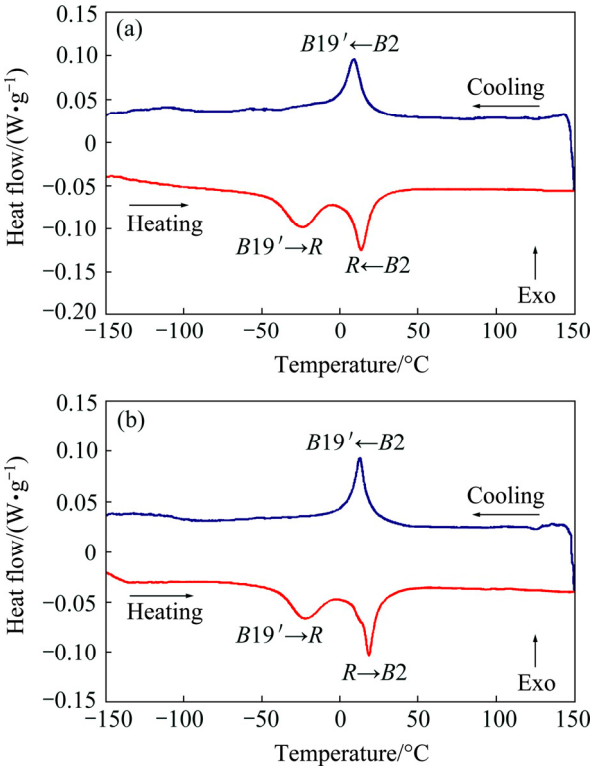

Fig. 8 DSC curves of 40% (a) and 70% (b) cold-rolled $Ti_{50}Ni_{48}Co_2$ specimens after annealing at 400 °C for 1 h

of martensite. Upon unloading, martensite is unloaded elastically and then the reverse transformation from martensite to austenite is observed, followed by elastic unloading of austenite.

Figure 10 summarizes the results extracted from Fig. 9, showing changes in the upper plateau stress (critical stress for stress-induced martensitic transformation) and the residual (irrecoverable) strain with increasing thickness reduction in cold rolling. It is observed that the stress level of the upper plateau (σ_{SIM}) significantly improved by increasing thickness reduction during cold rolling. It is noteworthy that in the 70% cold-rolled–annealed specimen, the value of σ_{SIM} was measured as high as 730 MPa which is significantly higher than that of the coarse-grained $Ti_{50}Ni_{48}Co_2$ (190 MPa) [13] and $Ni_{50}Ti_{50}$ (160 MPa) [25] alloys. Moreover, with increasing thickness reduction, the irrecoverable strain (ε_R) of $Ti_{50}Ni_{48}Co_2$ alloy was decreased during superelastic experiments such that the 70% cold-rolled–annealed specimens exhibited about 11% of recoverable strain which is significantly higher than that of the coarse-grained $Ni_{50}Ti_{50}$ shape memory alloy (~8%) [1].

The observed improvement in the superelastic behavior of the $Ti_{50}Ni_{48}Co_2$ alloy can be attributed to the enhancement of the critical dislocation-induced slip stress as a result of grain size reduction and formation of

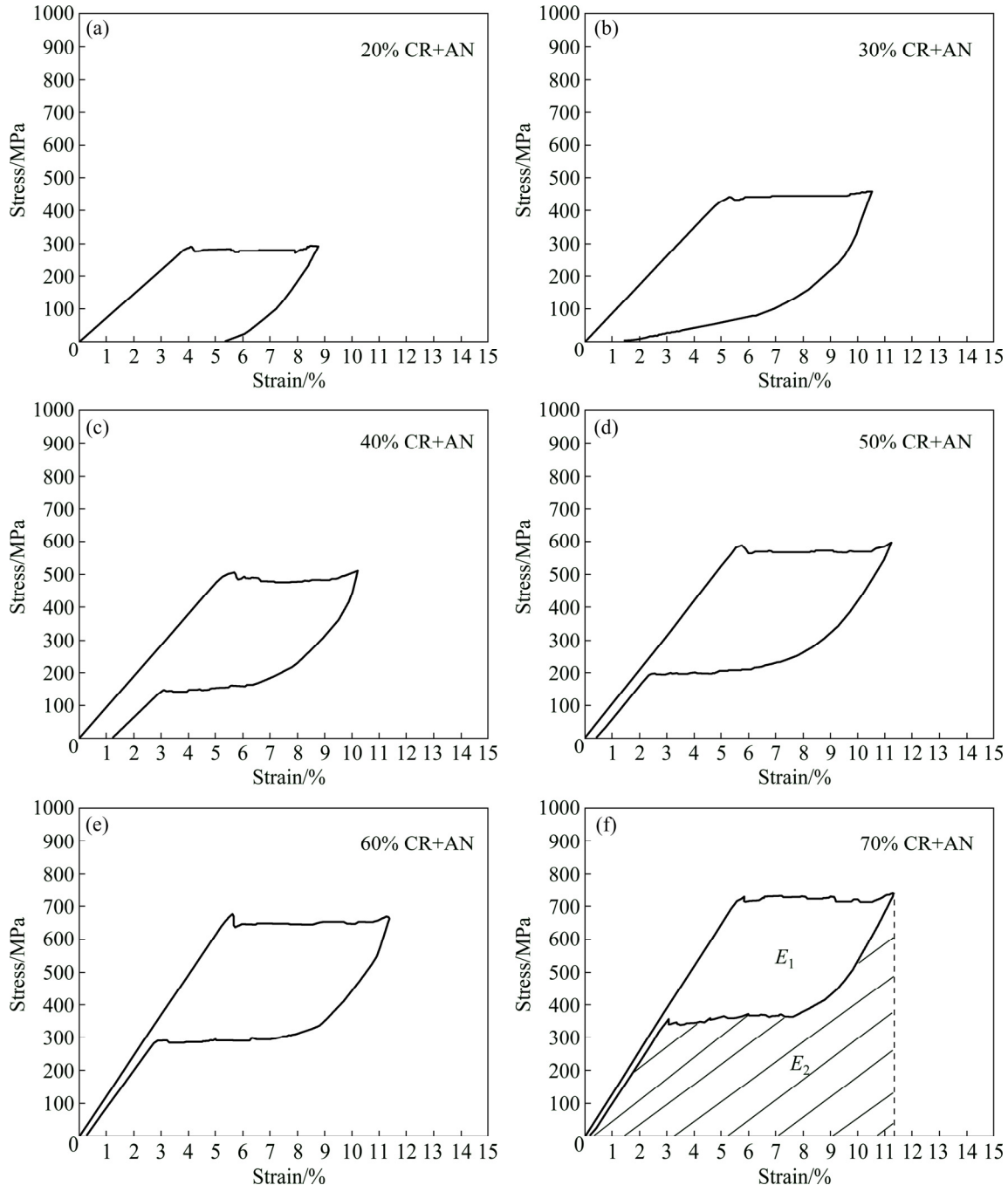

Fig. 9 Engineering tensile stress–strain curves of cold-rolled (CR) $Ti_{50}Ni_{48}Co_2$ specimens with various thickness reductions after annealing (AN) at 400 °C for 1 h

nanocrystalline structure [26]. As seen in Figs. 6 and 7, the annealed specimen with the higher thickness reduction (70%) had smaller grain size compared with the annealed specimen with lower thickness reduction (40%). The microstructure with smaller grin size provides a higher density of grain boundaries and the necessary strength to the austenite phase to avoid plastic deformation by slip mechanism and as a result stress-induced martensitic transformation could occur during tensile loading [27]. SHI et al [28] investigated the grain size effect on the stress hysteresis of a nanocrystalline NiTi alloy during superelastic cycling. They reported that the stress hysteresis of the samples after annealing was increased with decreasing grain size. Moreover, their results showed that the accumulation of dislocations affects the shape of the superelastic stress−strain curves. AHADI and SUN [29] investigated the effects of grain size on the rate-dependent thermomechanical responses of superelastic NiTi with an average grain size from 10 to 90 nm, under both

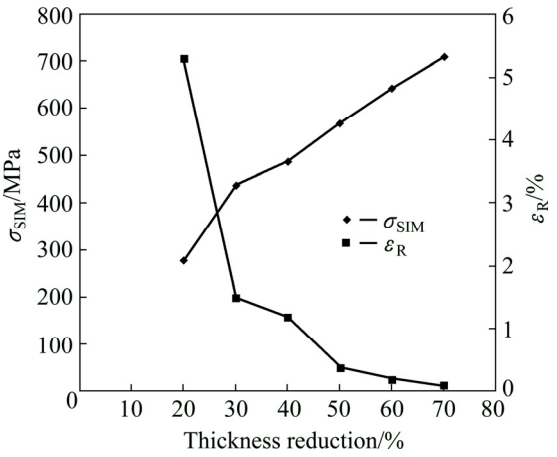

Fig. 10 Variations of upper plateau stress (σ_{SIM}) and residual strain (ε_R) versus applied thickness reduction for cold-rolled and annealed $Ti_{50}Ni_{48}Co_2$ specimens

monotonic and cyclic tensile loading–unloading. They found that with the grain size reduction to the nanoscale, the rate dependence of the transformation stress and the hysteresis loop area gradually were weakened and finally tended to vanish for a grain size of 10 nm.

The superelastic behavior has been used in a wide range of applications. Developers of vibration control devices in civil structures have shown interest in superelastic behavior of NiTi-based shape memory alloys due to their capabilities to dissipate energy through a large hysteresis. The origin of hysteresis in superelastic curves is related to the friction energy which originates from the austenite/martensite interface motion [30]. In Fig. 9, the area E_1 represents the energy density per unit volume which is dissipated during one complete cycle, while E_2 is the energy density per unit volume which is stored and available to release upon unloading. It is well known that the superelasticity characteristic can be applied for storing mechanical energy and the efficiency for the energy storage, η, can be defined as $E_2/(E_1+E_2)$ [31]. By comparing superelastic stress–strain curve of 70% cold-rolled specimen with others, it is easy to see that η increases with increasing cold-rolling (see Table 2). In other words, the cold rolling process could improve significantly energy storage efficiency of $Ti_{50}Ni_{48}Co_2$ alloy with increasing of σ_{SIM}.

Beside the high efficiency for the energy storage, the nanostructured $Ti_{50}Ni_{48}Co_2$ alloy has considerable damping capacity (E_D), which in simple terms is the ability to repeatedly disperse unwanted energy from a system. Damping capacity is related to the mechanical hysteresis and transformation strain and can be determined by calculating the area between the forward and reverse transformations in the superelastic stress–strain curves (E_D=E_1). High hysteresis and transformation strain result in more energy dissipation from a system [32]. Damping capacities of selected cold-rolled and annealed $Ti_{50}Ni_{48}Co_2$ specimens are compared in Table 2. It is noteworthy that in the 70% cold-rolled−annealed specimens, the value of E_D was measured to be 23 J/cm^3 which is significantly higher than that of commercial NiTi alloys (10 J/cm^3) [32]. So, because of their energy-absorbing capabilities, nanocrystalline $Ti_{50}Ni_{48}Co_2$ SMAs, could be employed as dampers in aerospace and construction industries.

Table 2 Average efficiency for energy storage (η) and damping capacities (E_D) of selected cold-rolled and annealed $Ti_{50}Ni_{48}Co_2$ specimens

Specimen	η/%	E_D/(J·cm^{-3})
50% CR+AN	57	20
60% CR+AN	61	22
70% CR+AN	64	23

4 Conclusions

1) The initial deformation mechanism of $Ti_{50}Ni_{48}Co_2$ alloy during cold rolling was stress-induced martensitic transformation followed by plastic deformation of martensite via dislocation slip and subsequent martensite to austenite transformation via the reverse transformation after unloading. By increasing the cold deformation, a high density of dislocations is accumulated, leading gradually to nanocrystallization and amorphization.

2) The calculated dislocation density of $Ti_{50}Ni_{48}Co_2$ alloy was increased to 8.55×10^{12} cm^{-2} with increasing thickness reduction up to 70%.

3) After annealing at 400 °C for 1h, the amorphous phase formed in the cold-rolled specimens was completely crystallized and a fully nanocrystalline structure was achieved in $Ti_{50}Ni_{48}Co_2$ alloy.

4) The grain size of the 40% cold-rolled and annealed specimen was 10−110 nm, whereas it was 5−60 nm for the 70% cold-rolled and annealed one. This could show the correlation between the final grain size and the thickness reduction during cold rolling prior to annealing treatment.

5) The stress level of the upper plateau (σ_{SIM}) of $Ti_{50}Ni_{48}Co_2$ alloy significantly improved by increasing thickness reduction during cold rolling. In the 70% cold-rolled−annealed specimen, the value of σ_{SIM} was measured as high as 730 MPa. Moreover, with increasing thickness reduction, the recoverable strain of $Ti_{50}Ni_{48}Co_2$ alloy was increased such that the 70% cold-rolled−annealed specimen exhibited about 11% of recoverable strain.

6) The observed improvement in the superelastic behavior of the $Ti_{50}Ni_{48}Co_2$ alloy could be attributed to

the enhancement of the critical dislocation-induced slip stress as a result of grain size reduction and formation of nanocrystalline structure

7) The nanocrystalline $Ti_{50}Ni_{48}Co_2$ alloy had a high damping capacity and considerable efficiency for energy storage. The damping capacity of the 70% cold-rolled−annealed specimen was measured to be 23 J/cm^3.

References

[1] OTSUKA K, WAYMAN C M. Shape memory materials [M]. Cambridge: Cambridge University Press, 1998.

[2] JIANG Shu-yong, ZHANG Yan-qiu. Microstructure evolution and deformation behavior of as-cast NiTi shape memory alloy under compression [J]. Transactions of Nonferrous Metals Society of China, 2012, 22: 90−96.

[3] TONG Yun-xiang, LIU Jun-ting, CHEN Feng, LIANG Chu-qi, TIAN Bing, LI Li, ZHENG Yu-feng. Effect of aging on martensitic transformation and superelasticity of TiNiCr shape memory alloy [J]. Transactions of Nonferrous Metals Society of China, 2014, 24: 2598−2605.

[4] LIU Y. The superelastic anisotropy in a NiTi shape memory alloy thin sheet [J]. Acta Mater, 2015, 95: 411−427.

[5] PROKOFIEV E, BUROW J, FRENZEL J, GUNDEROV D, EGGELER G, VALIEV R. Phase transformations and functional properties of NiTi alloy with ultrafine-grained structure [J]. Mater Sci Forum, 2011, 667−669: 1059−1064.

[6] RYKLINA E P, PROKOSHKIN S D, KREYTSBERG A Y. Abnormally high recovery strain in Ti−Ni-based shape memory alloys [J]. J Alloys Compd, 2013, 577: 255−258.

[7] JIANG Shu-yong, TANG Ming, ZHAO Ya-nan, HU Li, ZHANG Yan-qiu, LIANG Lu-long. Crystallization of amorphous NiTi shape memory alloy fabricated by severe plastic deformation [J]. Transactions of Nonferrous Metals Society of China, 2014, 24: 1758−1765.

[8] TSUCHIYA K, HADA Y, KOYANO T, NAKAJIMA K, OHNUMA M, KOIKE T, TODAKA Y, UMEMOTO M. Production of TiNi amorphous/nanocrystalline wires with high strength and elastic modulus by severe cold drawing [J]. Scripta Mater, 2009, 60: 749−752.

[9] DELVILLE R, MARALD B, PILCH J, SITTNER P, SCHRYVERS D. Microstructure changes during non-conventional heat treatment of thin Ni−Ti wires by pulsed electric current studied by transmission electron microscopy [J]. Acta Mater, 2010, 58: 4503−4515.

[10] MARALD B, PILCH J, SITTNER P, DELVILLE R, CURFS C. In situ investigation of the fast microstructure evolution during electropulse treatment of cold drawn NiTi wires [J]. Acta Mater, 2011, 59: 1542−1556.

[11] DRUGACZ J, LEKSTON Z, MORAWIEC H, JANUSZEWSKI K. Use of TiNiCo shape memory clamps in the surgical treatment of mandibular fractures [J]. J Oral Maxillofac Surg, 1995, 53: 665−671.

[12] FASCHING A, NORWICH D, GEISER T, PAUL G W. An evaluation of a NiTiCo alloy and its suitability for medical device applications. [J]. J Mater Eng Perform, 2011, 20: 641−645.

[13] JING Rui-rui, LIU Fu-shun. The influence of Co addition on phase transformation behavior and mechanical properties of TiNi alloys [J]. Chin [J]. J Aeronaut, 2007, 20: 153−156.

[14] MOHAMMAD SHARIFI E, KARIMZADEH F, KERMANPUR A. Nanocrystallization of the $Ti_{50}Ni_{48}Co_2$ shape memory alloy by thermomechanical treatment [J]. J Mater Eng Perform, 2015, 24: 445−451.

[15] MOHAMMAD SHARIFI E, KERMANPUR A, KARIMZADEH F. The effect of thermomechanical processing on the microstructure and mechanical properties of the nanocrystalline TiNiCo shape memory alloy [J]. Mater Sci Eng A, 2014, 598: 183−189.

[16] LUTTEROTTI L. MAUD: Materials Analysis Using Diffraction [EB/OL]. http//www.ing.unitn.it/~maud/.

[17] CHANDA A, DE M. X-ray characterization of the microstructure of α-CuTi alloys by Rietveld's method [J]. J Alloys Compd, 2000, 313: 104−114.

[18] MURUGESAN S, KUPPUSAMI P, MOHANDAS E, VIJAYALAKSHMI M. X-ray diffraction Rietveld analysis of cold worked austenitic stainless steel [J]. Mater Lett, 2012, 67: 173−176.

[19] SAHU P, DE M, KAJIWARA S. Microstructural characterization of stress-induced martensites evolved at low temperature in deformed powders of Fe−Mn−C alloys by the Rietveld method [J]. J Alloys Compd, 2002, 346: 158−169.

[20] DINI G, UEJI R, NAJAFIZADEH A, MONIR-VAGHEFI S M. Flow stress analysis of TWIP steel via the XRD measurement of dislocation density [J]. Mater Sci Eng A, 2010, 527: 2759−2763.

[21] TSUCHIYA K, INUZUKA M, TOMUS D, HOSOKAWA A, NAKAYAMA H, MORII K, TODAKA Y, UMEMOTO M. Martensitic transformation in nanostructured TiNi shape memory alloy formed via severe plastic deformation [J]. Mater Sci Eng A, 2006, 438−440: 643−648.

[22] PROKOSHKIN S D, KHMELEVSKAYA I Y, DOBATKIN S V, TRUBITSYNA I B, TATYANIN E V, STOLYAROV V V, PROKOFIEV E A. Alloy composition, deformation temperature, pressure and post-deformation annealing effects in severely deformed Ti−Ni based shape memory alloys [J]. Acta Mater, 2005, 53: 2703−2714.

[23] KOIKE J, PARKIN D M, NASTASI M. Crystal-to-amorphous transformation of NiTi induced by cold rolling [J]. J Mater Res, 1990, 7: 1414−1418.

[24] KARAMAN I, YAPICI G G, CHUMLYAKOV Y I, KIREEVA I V. Deformation twinning in difficult-to-work alloys during severe plastic deformation [J]. Mater Sci Eng A, 2005, 410−411: 243−247.

[25] TSUCHIYA K, CAO Q, HOSOKAWA A, KATAHIRA M, TODAKA Y, UMEMOTO M. Nanostructured shape memory alloys for biomedical applications [J]. Mater Sci Forum, 2007, 539−543: 505−510.

[26] ZHANG H, LI X, ZHANG X. Grain-size-dependent martensitic transformation in bulk nanocrystalline TiNi under tensile deformation [J]. J Alloys Compd, 2012, 544: 19−23.

[27] SAIKRISHNA C N, RAMAIAH K V, ALLAM PRABHU S, BHAUMIK S K. On stability of NiTi wire during thermo-mechanical cycling [J]. Bull Mater Sci, 2009, 32: 343−352.

[28] SHI X B, GUO F M, ZHANG J S, DING H L, CUI L S. Grain size effect on stress hysteresis of nanocrystalline NiTi alloys [J]. J Alloys Compd, 2016, 688: 62−68.

[29] AHADI A, SUN Q. Effects of grain size on the rate-dependent thermomechanical responses of nanostructured superelastic NiTi [J]. Acta Mater, 2014, 76: 186−197.

[30] MOHD JANI J, LEARY M, SUBIC A, GIBSON M A. A review of shape memory alloy research, applications and opportunities [J]. Mater Des, 2014, 56: 1078−1113.

[31] LIN H C, WU S K. The tensile behavior of a cold-rolled and reverse-transformed equiatomic TiNi alloy [J]. Acta Metal Mater, 1994, 42: 1623−1630.

[32] KARACA H E, ACAR E, DED G S, BASARAN B, TOBE H, NOEBE R D, BIGELOW G, CHUMLYAKOV Y I. Shape memory behavior of high strength NiTiHfPd polycrystalline alloys [J]. Acta Mater, 2013, 61: 5036−5049.

冷轧加工纳米结构 $Ti_{50}Ni_{48}Co_2$ 形状记忆合金的超弹性行为

E. MOHAMMAD SHARIFI[1], A. KERMANPUR[2]

1. Department of Materials Engineering, Malek Ashtar University of Technology, Shahin Shahr 83145115, Iran;
2. Department of Materials Engineering, Isfahan University of Technology, Isfahan 8415683111, Iran

摘　要：研究冷轧后退火对 $Ti_{50}Ni_{48}Co_2$ 形状记忆合金显微组织演化和超弹性性能的影响。结果表明，在冷轧制过程中，合金的显微组织经历了应力诱导马氏体相变和马氏体塑性变形、变形孪晶、马氏体中沿孪晶和不同晶界的位错堆积、纳米晶化、非晶化以及马氏体向奥氏体的可逆相变 6 个基本阶段。在 400 °C 退火 1 h 后, 冷轧样品中形成的非晶相完全晶化，生成了一个完全纳米晶体的结构。这种纳米晶体合金的峰应力高达 730 MPa，明显高于粗晶 $Ni_{50}Ti_{50}$ 和 $Ti_{50}Ni_{48}Co_2$ 合金。而且，纳米晶 $Ti_{50}Ni_{48}Co_2$ 合金具有较高的阻尼容量和较好的储能效率。

关键词：形状记忆合金；超弹性；纳米晶材料；热机械加工

(Edited by Xiang-qun LI)